The Astrophysical Journal Letters, 867:L19 (8pp), 2018 November 1 https://doi.org/10.3847/2041-8213/aae70e

Periastron Observations of TeV Gamma-Ray Emission from a Binary System with a 50-year Period

A. U. Abeysekara[1], W. Benbow[2], R. Bird[3], A. Brill[4], R. Brose[5,6], J. H. Buckley[7], A. J. Chromey[8], M. K. Daniel[2], A. Falcone[9], J. P. Finley[10], L. Fortson[11], A. Furniss[12], A. Gent[13], G. H. Gillanders[14], D. Hanna[15], T. Hassan[6], O. Hervet[16], J. Holder[17], G. Hughes[2], T. B. Humensky[4], P. Kaaret[18], P. Kar[1], M. Kertzman[19], D. Kieda[1], M. Krause[6], F. Krennrich[8], S. Kumar[15,17], M. J. Lang[14], T. T. Y. Lin[15], G. Maier[6], P. Moriarty[14], R. Mukherjee[20], S. O'Brien[21], R. A. Ong[3], A. N. Otte[13], N. Park[22], A. Petrashyk[4], M. Pohl[5,6], E. Pueschel[6], J. Quinn[21], K. Ragan[15], G. T. Richards[13,17], E. Roache[2], I. Sadeh[6], M. Santander[23], S. Schlenstedt[6], G. H. Sembroski[10], I. Sushch[6], J. Tyler[15], V. V. Vassiliev[3], S. P. Wakely[24], A. Weinstein[8], R. M. Wells[8], P. Wilcox[18], A. Wilhelm[5,6], D. A. Williams[16], T J Williamson[17], B. Zitzer[15]

(VERITAS Collaboration),

and

V. A. Acciari[25], S. Ansoldi[26,27], L. A. Antonelli[28], A. Arbet Engels[29], D. Baack[30], A. Babić[31], B. Banerjee[32], U. Barres de Almeida[33], J. A. Barrio[34], J. Becerra González[25], W. Bednarek[35], E. Bernardini[36,37], A. Berti[38,39], J. Besenrieder[40], W. Bhattacharyya[36], C. Bigongiari[28], A. Biland[29], O. Blanch[41], G. Bonnoli[42], G. Busetto[43], R. Carosi[44], G. Ceribella[40], S. Cikota[31], S. M. Colak[41], P. Colin[40], E. Colombo[25], J. L. Contreras[34], J. Cortina[41], S. Covino[28], V. D'Elia[28], P. Da Vela[44], F. Dazzi[28], A. De Angelis[43], B. De Lotto[26], M. Delfino[41,45], J. Delgado[41,45], F. Di Pierro[39], E. Do Souto Espiñera[41], A. Domínguez[34], D. Dominis Prester[31], D. Dorner[46], M. Doro[43], S. Einecke[30], D. Elsaesser[30], V. Fallah Ramazani[47], A. Fattorini[30], A. Fernández-Barral[43], G. Ferrara[28], D. Fidalgo[34], L. Foffano[43], M. V. Fonseca[34], L. Font[48], C. Fruck[40], D. Galindo[49], S. Gallozzi[28], R. J. García López[25], M. Garczarczyk[36], S. Gasparyan[50], M. Gaug[48], P. Giammaria[28], N. Godinović[31], D. Guberman[41], D. Hadasch[27], A. Hahn[40], J. Herrera[25], J. Hoang[34], D. Hrupec[31], S. Inoue[27], K. Ishio[40], Y. Iwamura[27], H. Kubo[27], J. Kushida[27], D. Kuveždić[31], A. Lamastra[28], D. Lelas[31], F. Leone[28], E. Lindfors[47], S. Lombardi[28], F. Longo[26,38], M. López[34], A. López-Oramas[25], B. Machado de Oliveira Fraga[33], C. Maggio[48], P. Majumdar[32], M. Makariev[51], M. Mallamaci[43], G. Maneva[51], M. Manganaro[31], K. Mannheim[46], L. Maraschi[28], M. Mariotti[43], M. Martínez[41], S. Masuda[27], D. Mazin[40,27], M. Minev[51], J. M. Miranda[42], R. Mirzoyan[40], E. Molina[49], A. Moralejo[41], V. Moreno[48], E. Moretti[41], P. Munar-Adrover[48], V. Neustroev[47], A. Niedzwiecki[35], M. Nievas Rosillo[34], C. Nigro[36], K. Nilsson[47], D. Ninci[41], K. Nishijima[27], K. Noda[27], L. Nogués[41], M. Nöthe[30], S. Paiano[43], J. Palacio[41], D. Paneque[40], R. Paoletti[42], J. M. Paredes[49], G. Pedaletti[36], P. Peñil[34], M. Peresano[26], M. Persic[26,52], P. G. Prada Moroni[44], E. Prandini[43], I. Puljak[31], J. R. Garcia[40], W. Rhode[30], M. Ribó[49], J. Rico[41], C. Righi[28], A. Rugliancich[44], L. Saha[34], N. Sahakyan[50], T. Saito[27], K. Satalecka[36], T. Schweizer[40], J. Sitarek[35], I. Šnidarić[31], D. Sobczynska[35], A. Somero[25], A. Stamerra[28], M. Strzys[40], T. Surić[31], F. Tavecchio[28], P. Temnikov[51], T. Terzić[31], M. Teshima[40,27], N. Torres-Albà[49], S. Tsujimoto[27], J. van Scherpenberg[40], G. Vanzo[25], M. Vazquez Acosta[25], I. Vovk[40], M. Will[40], and D. Zarić[31]

(MAGIC Collaboration)

[1] Department of Physics and Astronomy, University of Utah, Salt Lake City, UT 84112, USA
[2] Fred Lawrence Whipple Observatory, Harvard-Smithsonian Center for Astrophysics, Amado, AZ 85645, USA
[3] Department of Physics and Astronomy, University of California, Los Angeles, CA 90095, USA; ralphbird@astro.ucla.edu
[4] Physics Department, Columbia University, New York, NY 10027, USA
[5] Institute of Physics and Astronomy, University of Potsdam, D-14476 Potsdam-Golm, Germany
[6] DESY, Platanenallee 6, D-15738 Zeuthen, Germany
[7] Department of Physics, Washington University, St. Louis, MO 63130, USA
[8] Department of Physics and Astronomy, Iowa State University, Ames, IA 50011, USA
[9] Department of Astronomy and Astrophysics, 525 Davey Lab, Pennsylvania State University, University Park, PA 16802, USA
[10] Department of Physics and Astronomy, Purdue University, West Lafayette, IN 47907, USA
[11] School of Physics and Astronomy, University of Minnesota, Minneapolis, MN 55455, USA
[12] Department of Physics, California State University—East Bay, Hayward, CA 94542, USA
[13] School of Physics and Center for Relativistic Astrophysics, Georgia Institute of Technology, 837 State Street NW, Atlanta, GA 30332-0430, USA
[14] School of Physics, National University of Ireland Galway, University Road, Galway, Ireland
[15] Physics Department, McGill University, Montreal, QC H3A 2T8, Canada
[16] Santa Cruz Institute for Particle Physics and Department of Physics, University of California, Santa Cruz, CA 95064, USA
[17] Department of Physics and Astronomy and the Bartol Research Institute, University of Delaware, Newark, DE 19716, USA; tjwilli@udel.edu
[18] Department of Physics and Astronomy, University of Iowa, Van Allen Hall, Iowa City, IA 52242, USA
[19] Department of Physics and Astronomy, DePauw University, Greencastle, IN 46135-0037, USA
[20] Department of Physics and Astronomy, Barnard College, Columbia University, NY 10027, USA
[21] School of Physics, University College Dublin, Belfield, Dublin 4, Ireland
[22] WIPAC and Department of Physics, University of Wisconsin-Madison, Madison, WI, USA
[23] Department of Physics and Astronomy, University of Alabama, Tuscaloosa, AL 35487, USA
[24] Enrico Fermi Institute, University of Chicago, Chicago, IL 60637, USA
[25] Inst. de Astrofísica de Canarias, E-38200 La Laguna, and Universidad de La Laguna, Dpto. Astrofísica, E-38206 La Laguna, Tenerife, Spain jaherllo@iac.es, aloramas@iac.es
[26] Università di Udine, and INFN Trieste, I-33100 Udine, Italy

[27] Japanese MAGIC Consortium: ICRR, The University of Tokyo, 277-8582 Chiba, Japan; Department of Physics, Kyoto University, 606-8502 Kyoto, Japan; Tokai University, 259-1292 Kanagawa, Japan; RIKEN, 351-0198 Saitama, Japan
[28] National Institute for Astrophysics (INAF), I-00136 Rome, Italy
[29] ETH Zurich, CH-8093 Zurich, Switzerland
[30] Technische Universität Dortmund, D-44221 Dortmund, Germany
[31] Croatian MAGIC Consortium: University of Rijeka, 51000 Rijeka, Croatia; University of Split—FESB, 21000 Split, Croatia; University of Zagreb—FER, 10000 Zagreb, Croatia; University of Osijek, 31000 Osijek, Croatia; Rudjer Boskovic Institute, 10000 Zagreb, Croatia
[32] Saha Institute of Nuclear Physics, HBNI, 1/AF Bidhannagar, Salt Lake, Sector-1, Kolkata 700064, India
[33] Centro Brasileiro de Pesquisas Físicas (CBPF), 22290-180 URCA, Rio de Janeiro (RJ), Brasil
[34] Unidad de Partículas y Cosmología (UPARCOS), Universidad Complutense, E-28040 Madrid, Spain
[35] University of Łódź, Department of Astrophysics, PL-90236 Łódź, Poland
[36] Deutsches Elektronen-Synchrotron (DESY), D-15738 Zeuthen, Germany
[37] Humboldt University of Berlin, Institut für Physik D-12489 Berlin, Germany
[38] Dipartimento di Fisica, Università di Trieste, I-34127 Trieste, Italy
[39] Istituto Nazionale Fisica Nucleare (INFN), I-00044 Frascati (Roma) Italy
[40] Max-Planck-Institut für Physik, D-80805 München, Germany
[41] Institut de Física d'Altes Energies (IFAE), The Barcelona Institute of Science and Technology (BIST), E-08193 Bellaterra (Barcelona), Spain
[42] Università di Siena and INFN Pisa, I-53100 Siena, Italy
[43] Università di Padova and INFN, I-35131 Padova, Italy
[44] Università di Pisa, and INFN Pisa, I-56126 Pisa, Italy
[45] Port d'Informació Científica (PIC) E-08193 Bellaterra (Barcelona), Spain
[46] Universität Würzburg, D-97074 Würzburg, Germany
[47] Finnish MAGIC Consortium: Tuorla Observatory (Department of Physics and Astronomy) and Finnish Centre of Astronomy with ESO (FINCA), University of Turku, FI-20014 Turku, Finland; Astronomy Division, University of Oulu, FI-90014 Oulu, Finland
[48] Departament de Física, and CERES-IEEC, Universitat Autònoma de Barcelona, E-08193 Bellaterra, Spain
[49] Universitat de Barcelona, ICCUB, IEEC-UB, E-08028 Barcelona, Spain
[50] ICRAN Net-Armenia at NAS RA, 0019 Yerevan, Armenia
[51] Inst. for Nucl. Research and Nucl. Energy, Bulgarian Academy of Sciences, BG-1784 Sofia, Bulgaria
[52] INAF-Trieste and Dept. of Physics & Astronomy, University of Bologna

Received 2018 August 20; revised 2018 October 1; accepted 2018 October 9; published 2018 October 31

Abstract

We report on observations of the pulsar/Be star binary system PSR J2032+4127/MT91 213 in the energy range between 100 GeV and 20 TeV with the Very Energetic Radiation Imaging Telescope Array and Major Atmospheric Gamma Imaging Cherenkov telescope arrays. The binary orbit has a period of approximately 50 years, with the most recent periastron occurring on 2017 November 13. Our observations span from 18 months prior to periastron to one month after. A new point-like gamma-ray source is detected, coincident with the location of PSR J2032+4127/MT91 213. The gamma-ray light curve and spectrum are well characterized over the periastron passage. The flux is variable over at least an order of magnitude, peaking at periastron, thus providing a firm association of the TeV source with the pulsar/Be star system. Observations prior to periastron show a cutoff in the spectrum at an energy around 0.5 TeV. This result adds a new member to the small population of known TeV binaries, and it identifies only the second source of this class in which the nature and properties of the compact object are firmly established. We compare the gamma-ray results with the light curve measured with the X-ray Telescope on board the Neil Gehrels *Swift* Observatory and with the predictions of recent theoretical models of the system. We conclude that significant revision of the models is required to explain the details of the emission that we have observed, and we discuss the relationship between the binary system and the overlapping steady extended source, TeV J2032+4130.

Key words: gamma rays: general – pulsars: individual (PSR J2032+4127, VER J2032+414, MAGIC J2032+4127) – stars: individual (MT91 213) – X-rays: binaries

1. Introduction

TeV gamma-ray emitting binary systems are extremely rare objects, likely corresponding to a relatively brief period in the evolution of some massive star binaries (Dubus et al. 2017). They consist of a neutron star or black hole in a binary orbit with a massive star, and their high-energy emission provides a unique opportunity to study relativistic particle acceleration in a continuously changing physical environment. Of particular interest are systems where the compact object is a pulsar, as the pulsed emission firmly identifies the nature of the compact object and provides an accurate determination of the orbital parameters, the available energy budget, and the likely acceleration mechanism. Prior to this Letter, only one TeV binary with a known pulsar had been detected: the pulsar/Be star binary system PSR B1259–63/LS 2883 (Aharonian et al. 2005). In this Letter, we present the discovery of a second member of this class, PSR J2032+4127/MT91 213.

Pulsed emission, with a period of $P = 143$ ms, was first detected from PSR J2032+4127 in a blind search of *Fermi*-Large Area Telescope (LAT) gamma-ray data (Abdo et al. 2009) and was subsequently detected in radio observations with the Green Bank Telescope (GBT; Camilo et al. 2009). These observations revealed dramatic changes in the pulsar spin-down rate, an effect most easily explained by Doppler shift due to the pulsar's motion in a long-period binary system (Lyne et al. 2015). The pulsar's companion was identified as a B0Ve star, MT91 213, which has a mass of around 15 $M_\odot$ and a circumstellar disk that varies in radius by more than a factor of two, from 0.2 to 0.5 au (Ho et al. 2017). The pulsar spin-down luminosity ($\dot{E}$) is 1.7×10^{35} erg s^{-1}, with a characteristic age of 180 kyr, and the system lies at a distance of 1.4–1.7 kpc, in the Cyg OB2 stellar association. Further observations refined the orbital parameters, yielding a binary period of 45–50 years, an eccentricity between 0.94 and 0.99, and a longitude of periastron between 21° and 52°. Periastron occurred on 2017 November 13 with a separation between PSR J2032+4127 and MT91 213 of approximately 1 au (Coe et al. 2017; Ho et al. 2017).

Significant X-ray brightening from the direction of PSR J2032+4127 was first detected by Ho et al. (2017), with the X-ray flux increasing by a factor of twenty relative to 2010 measurements. Li et al. (2017) used data from *Chandra*, *Swift*-X-Ray Telescope (XRT), *NuSTAR*, and *XMM-Newton* to conduct a detailed study of the long-term light curve, finding variability on timescales of weeks on top of the long-term increasing trend, which they attributed to clumps in the stellar wind. The structure of the stellar wind was further explored by Petropoulou et al. (2018), who used *Swift*-XRT observations to map the circumstellar environment of the Be star. Recently, Li et al. (2018) presented detailed *Swift*, *Fermi*-LAT, and radio observations of PSR J2032+4127 over the 2017 periastron period. They report strong variability in the X-ray flux, but no variability in the GeV gamma-ray flux, likely because this is masked by magnetospheric emission from the pulsar.

PSR J2032+4127 lies at the edge of the steady, extended, very-high-energy (VHE; $E > 100$ GeV) gamma-ray source, TeV J2032+4130. This object was the first VHE source to be serendipitously discovered, by the High-Energy-Gamma-Ray Astronomy telescope (HEGRA; Aharonian et al. 2002), and was not associated with any counterpart at other wavelengths. Subsequent observations by HEGRA and the Major Atmospheric Gamma Imaging Cherenkov (MAGIC) telescope arrays revealed an extended object, with a width of approximately 6′ and a hard power-law spectrum ($\Gamma \sim 2.0$) (Aharonian et al. 2005; Albert et al. 2008a). Very Energetic Radiation Imaging Telescope Array (VERITAS) observations have shown that the extended emission is asymmetric and coincident with a void in radio emission (Aliu et al. 2014). Prior to the discovery of its binary nature, an association of TeV J2032+4130 with the pulsar wind nebula (PWN) of PSR J2032+4127 seemed the most likely origin for the VHE source.

Thus far, only a handful of VHE gamma-ray emitting binary systems have been detected, of which only PSR B1259–63/LS 2883 has an identified compact object: a pulsar in a highly elliptical ($e = 0.87$) orbit with a period of 3.4 years and a periastron separation of about 1 au (Johnston et al. 1992; Negueruela et al. 2011). The unpulsed radio, X-ray, and VHE gamma-ray fluxes show complex light curves, with the majority of the emission occurring close to periastron in two distinct peaks, likely related to the pulsar passage through the circumstellar decretion disk. High-energy (HE; 0.1 GeV $< E <$ 100 GeV) emission, conversely, is generally weak around periastron, followed by intense flaring episodes that occur typically more than 30, and as long as 70, days after periastron (Abdo et al. 2011; Johnson et al. 2018).

In this Letter, we report on the results of extensive VHE gamma-ray observations of the 2017 periastron passage of the PSR J2032+4127/MT91 213 system using VERITAS and MAGIC, as well as presenting contemporaneous X-ray observations with *Swift*-XRT.

2. Observations and Analysis

VHE gamma-ray observations of PSR J2032+4127/MT91 213 were conducted by MAGIC and VERITAS, which are sensitive to astrophysical gamma-rays above 50 GeV. MAGIC consists of two 17 m diameter telescopes, located at the observatory of El Roque de Los Muchachos on the island of La Palma, Spain, whereas VERITAS is an array of four 12 m diameter telescopes at the Fred Lawrence Whipple Observatory near Tucson, Arizona. The observatories and their capabilities are described in Aleksić et al. (2016; MAGIC) and Park et al. (2015; VERITAS), and references therein.

In this Letter, we present the results of 181.3 hr of observations with VERITAS (51.6 hr of archival data taken before 2016, 30.1 hr between 2016 September and 2017 June, 99.6 hr between 2017 September and December) and 87.9 hr of observations with MAGIC (53.7 hr between 2016 May and September and 34.2 hr between 2017 June and December). Observations were conducted in “wobble” mode, with the source location offset from the center of the field of view, allowing simultaneous evaluation of the background (Fomin et al. 1994). The data were analyzed using standard tools (Zanin et al. 2013; Maier & Holder 2017), in which Cherenkov images are first calibrated, cleaned, and parameterized (Hillas 1985), then used to reconstruct the energy and arrival direction of the incident gamma-ray, and to reject the majority of the cosmic-ray background (Krawczynski et al. 2006; Albert et al. 2008b).

A total of 186 *Swift*-XRT (Burrows et al. 2005) observations were taken between 2008 June 16 and 2018 April 15, equating to 136.4 hr of live time. The data were collected in photon-counting mode and analyzed using the HEAsoft analysis package version 6.24.[53] The background was estimated from five regions equidistant from PSR J2032+4127, and the flux was calculated using XSPEC.

3. Variability, Morphology, and Spectrum

A new spatially unresolved time-varying VHE gamma-ray source was detected at a position compatible with PSR J2032+4127/MT91 213. The source is named VER J2032+414 and MAGIC J2032+4127 in the VERITAS and MAGIC source catalogs, respectively. It is also spatially coincident with TeV J2032+4130, the previously detected extended VHE source, but offset from the centroid of the extended emission by approximately 10′.

The complete X-ray and gamma-ray light curves are shown in Figure 1. Following the initial detection of PSR J2032+4127/MT91 213 in 2017 September by VERITAS and MAGIC (VERITAS & MAGIC Collaborations 2017) with a flux exceeding the baseline flux from TeV J2032+4130, gamma-ray emission was observed to increase up to the time of periastron (2017 November 13; MJD 58070), reaching a factor of 10 higher than the baseline. Approximately one week after periastron the flux sharply decreased to a level compatible with the baseline emission, before recovering to the periastron level a few days later. Further observations were conducted after periastron, but the combination of low source elevation angle, poor weather conditions, and rather brief exposure resulted in a relatively poor flux measurement. In total, during the 2017 fall observations (MJD 57997–58110), VERITAS

[53] https://heasarc.nasa.gov/lheasoft/

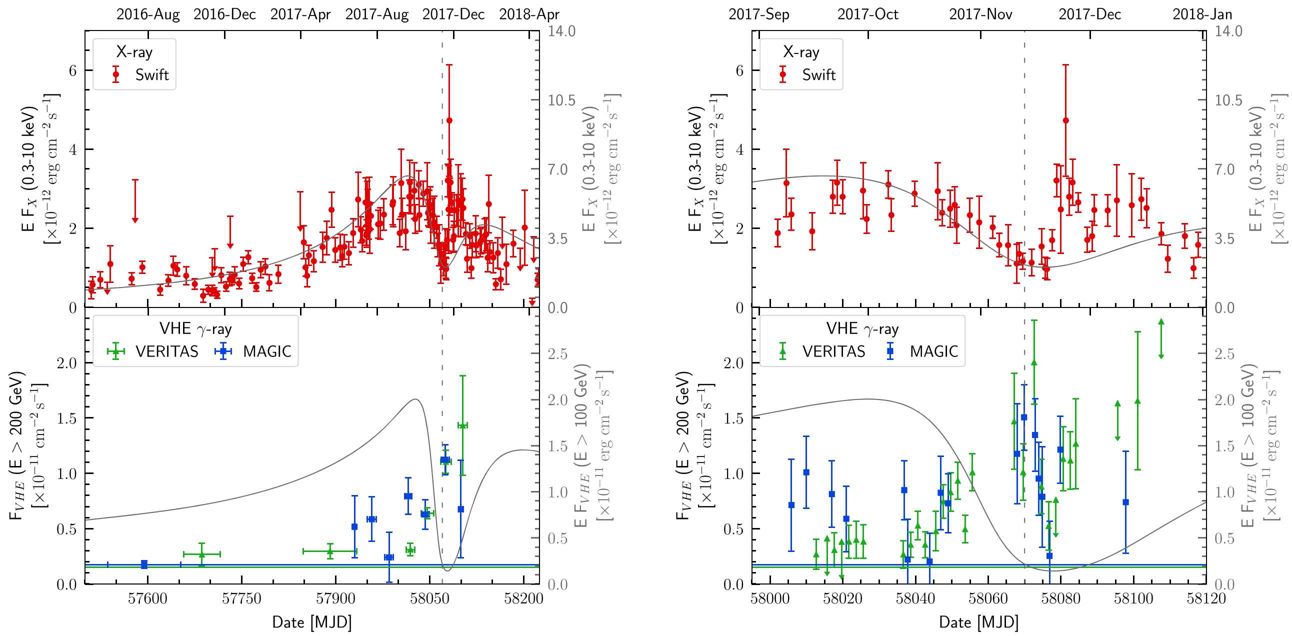

(a) Full Dataset (b) Periastron

Figure 1. Upper panels (left axes) show the 0.3–10.0 keV background-subtracted *Swift*-XRT energy-flux light curve (red circles) of PSR J2032+4127/MT91 213. For clarity, observations with exposures less than 1.4 ks are excluded from the plot. Lower panels show the >200 GeV photon-flux light curves from VERITAS (green triangles) and MAGIC (blue squares). The left plot shows the full light curve, while the right plot shows only the months around periastron. The horizontal solid lines indicate the average flux prior to 2017 for the respective experiments. The solid gray lines (right axes) are the energy-flux light curve predictions from Li et al. (2018) for X-rays and updated predictions from Takata et al. (2017) using the parameters from Li et al. (2018; J. Takata 2018, private communication) for VHE gamma-rays. Both models assume an inclination angle of 60°. The vertical gray dashed line indicates periastron.

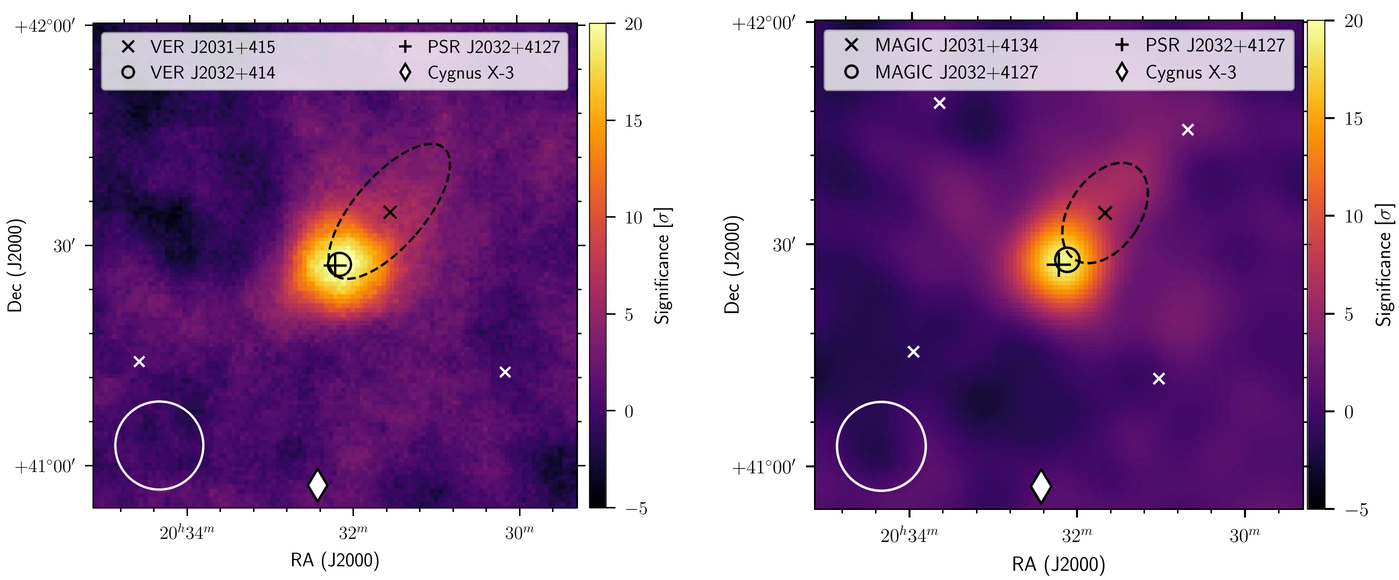

(a) (b)

Figure 2. Significance sky maps of the region around PSR J2032+4127/MT91 213 showing both the VERITAS (left panel) and MAGIC (right panel) results for observations during 2017 fall. The position of PSR J2032+4127/MT91 213 is shown as a black "+," the centroid of the gamma-ray emission as a black "∘," the position and extension for the respective telescope's measurements of TeV J2032+4130 are shown as a black "×" and a dashed line, and the position of Cygnus X-3 is shown with a white diamond. The white circle in the lower left-hand corner is of radius 0°.1, the approximate point-spread function for these measurements at 1 TeV. The wobble positions are shown as white "×."

detected PSR J2032+4127/MT91 213 with a significance of 21.5 standard deviations (σ) and MAGIC with a significance of 19.5σ.

Figure 2 shows sky maps for the complete fall 2017 VHE data sets, revealing overlapping emission from TeV J2032+4130 and PSR J2032+4127/MT91 213. For both the VERITAS and MAGIC data we fit the gamma-ray excess maps with a two-component model, consisting of a bivariate Gaussian function to represent the extended source and a symmetrical Gaussian function to model the unresolved emission at the location of the binary. The parameters of the extended source model, indicated by the dashed ellipses in

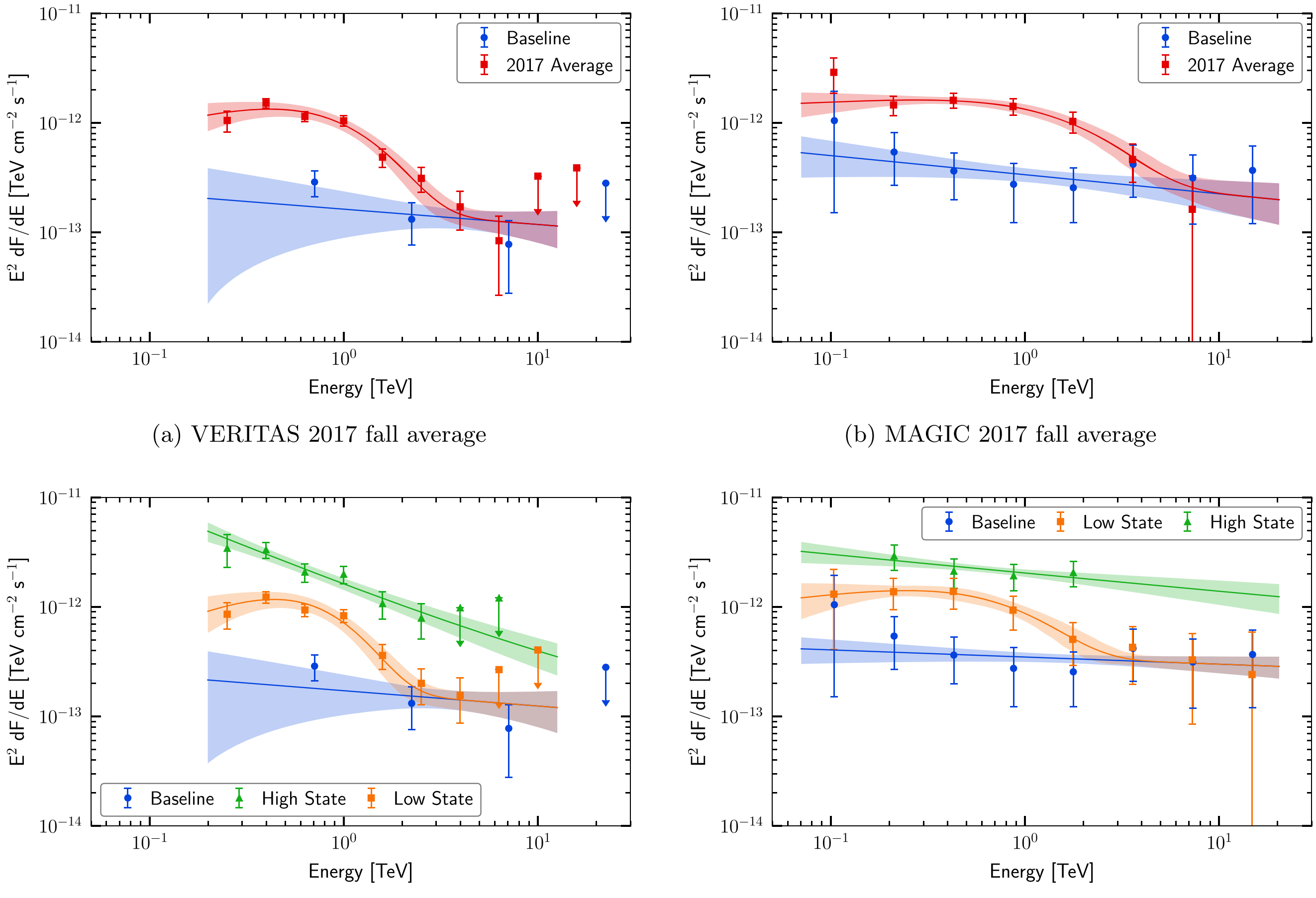

(a) VERITAS 2017 fall average

(b) MAGIC 2017 fall average

(c) VERITAS high & low states

(d) MAGIC high & low states

Figure 3. Spectral energy distributions for PSR J2032+4127/MT91 213 and TeV J2032+4130 from VERITAS (left) and MAGIC (right). The blue butterflies are the spectral fits to TeV J2032+4130. The red butterflies in the upper plots are fits to the 2017 fall data: the sum of a power-law fit to TeV J2032+4130 and a cutoff power-law fit to PSR J2032+4127/MT91 213. In the bottom plots, orange is the fit to the low-state data (PSR J2032+4127/MT91 213 is fit with a cutoff), while green represents the high-state data (PSR J2032+4127/MT91 213 is fit with a power law). The fit parameters are given in Table 1 and the time periods are defined in the text.

Figure 2, were constrained to match those measured prior to the appearance of the binary. For MAGIC, the extended source has a semimajor axis of $0^{\circ}.125 \pm 0^{\circ}.01$ and a semiminor axis of $0^{\circ}.08 \pm 0^{\circ}.01$, centered on R.A. $= 20^{\mathrm{h}}31^{\mathrm{m}}39.7^{\mathrm{s}} \pm 2^{\mathrm{s}}$, decl. $= 41^{\circ}34'23'' \pm 20''$, at an angle of $34^{\circ} \pm 2^{\circ}$ east of north. For VERITAS, the extended source parameters are those reported in Abeysekara et al. (2018): semimajor and semiminor axes of $0^{\circ}.19 \pm 0^{\circ}.02_{\mathrm{stat}} \pm 0^{\circ}.01_{\mathrm{sys}}$ and $0^{\circ}.08 \pm 0^{\circ}.01_{\mathrm{stat}} \pm 0^{\circ}.03_{\mathrm{sys}}$, centered on R.A. $= 20^{\mathrm{h}}31^{\mathrm{m}}33^{\mathrm{s}} \pm 2^{\mathrm{s}}_{\mathrm{stat}} \pm 2^{\mathrm{s}}_{\mathrm{sys}}$, decl. $= 41^{\circ}\ 34'\ 38'' \pm 36''_{\mathrm{stat}} \pm 36''_{\mathrm{sys}}$, with an orientation of $41^{\circ} \pm 4^{\circ}_{\mathrm{stat}} \pm 1^{\circ}_{\mathrm{sys}}$ east of north. The centroid of the unresolved component is measured to be at R.A. $= 20^{\mathrm{h}}32^{\mathrm{m}}10^{\mathrm{s}} \pm 2^{\mathrm{s}}_{\mathrm{stat}} \pm 2^{\mathrm{s}}_{\mathrm{sys}}$, decl. $= 41^{\circ}27'34'' \pm 16''_{\mathrm{stat}} \pm 26''_{\mathrm{sys}}$ for VERITAS, and R.A. $= 20^{\mathrm{h}}32^{\mathrm{m}}7^{\mathrm{s}} \pm 2^{\mathrm{s}}_{\mathrm{stat}}$, decl. $= 41^{\circ}28'4'' \pm 20''_{\mathrm{stat}}$ for MAGIC, which are consistent, within the measured uncertainties, with the location of PSR J2032+4127/MT91 213 ($20^{\mathrm{h}}32^{\mathrm{m}}\ 13^{\mathrm{s}}.12 \pm 0^{\mathrm{s}}.02 + 41^{\circ}27'24''.34 \pm 0''.03$; Gaia Collaboration 2018).

The source spectrum (Figure 3) is also formed of two emission components: steady, baseline emission from the extended source TeV J2032+4130 and variable emission associated with the binary system. Prior to 2017, only the baseline emission component was present, while the 2017 data include contributions from both the baseline and the variable binary. We performed a global spectral fit to the complete data set, in which the pre-2017 observations were fit with a pure power law for the baseline, and the 2017 data were fit with the same power law, plus an additional component for the binary emission. Two models were tested for the binary emission: a pure power law and a power law with an exponential cutoff. The VERITAS data favor the cutoff model over the power law for the binary emission, with an F-test probability of 0.997 and a cutoff energy of 0.57 ± 0.20 TeV. MAGIC observations also favor an exponential cutoff, with a probability of 0.993 and a cutoff energy of 1.40 ± 0.97 TeV. Full details of the fit parameters are given in Table 1. We note that the only other gamma-ray binary to display a spectral cutoff in the VHE regime is LS 5039, with a cutoff at 8.7 ± 2.0 TeV in the VHE high state, close to inferior conjunction (Aharonian et al. 2006).

The fit process was then repeated with the 2017 data broken up into two periods, to search for spectral variation with orbital phase and/or flux state of the binary system. We define a high state (MJD 58057–58074 and 58080–58110), which covers the periods around periastron where the flux above 0.2 TeV was greater than $1.0 \times 10^{-11}\ \mathrm{cm}^{-2}\ \mathrm{s}^{-1}$ (approximately five times greater than the baseline flux from TeV J2032+4130), and a low state, covering the 2017 observations prior to periastron (MJD 57928–58056). We performed a global fit to the data

Table 1
VHE Gamma-Ray Spectral Fit Results

	Period	Model Components	N_0 ($\mathrm{cm}^{-2}\ \mathrm{s}^{-1}\ \mathrm{TeV}^{-1}$)	E_0 (TeV)	Γ	E_C (TeV)	χ^2/dof
VERITAS (>220 GeV)	Pre-2017	$\mathbf{PL}_{\mathrm{baseline}}$	$(8.78 \pm 2.56) \times 10^{-15}$	3.47	2.14 ± 0.53	⋯	40.6/7
	Fall 2017	$\mathrm{PL}_{\mathrm{baseline}} + \mathbf{PL}_{\mathrm{binary}}$	$(1.53 \pm 0.14) \times 10^{-12}$	0.70	2.81 ± 0.09	⋯	
	Pre-2017	$\mathbf{PL}_{\mathrm{baseline}}$	$(7.62 \pm 1.51) \times 10^{-15}$	4.18	2.14 ± 0.29	⋯	8.6/6
	Fall 2017	$\mathrm{PL}_{\mathrm{baseline}} + \mathbf{PLEC}_{\mathrm{binary}}$	$(8.04 \pm 3.37) \times 10^{-12}$	0.64	1.26 ± 0.45	0.57 ± 0.20	
	Pre-2017	$\mathbf{PL}_{\mathrm{baseline}}$	$(4.65 \pm 1.18) \times 10^{-15}$	4.98	2.14 ± 0.85	⋯	26.8/10
	Low State	$\mathrm{PL}_{\mathrm{baseline}} + \mathbf{PL}_{\mathrm{binary}}$	$(8.12 \pm 3.77) \times 10^{-14}$	1.76	2.86 ± 0.11	⋯	
	High State	$\mathrm{PL}_{\mathrm{baseline}} + \mathbf{PL}_{\mathbf{binary}}$	$(9.69 \pm 1.75) \times 10^{-13}$	1.17	2.72 ± 0.15	⋯	
	Pre-2017	$\mathbf{PL}_{\mathrm{baseline}}$	$(1.23 \pm 0.24) \times 10^{-14}$	3.43	2.14 ± 0.28	⋯	7.9/9
	Low State	$\mathrm{PL}_{\mathrm{baseline}} + \mathbf{PLEC}_{\mathrm{binary}}$	$(1.63 \pm 1.12) \times 10^{-11}$	0.56	0.65 ± 0.75	0.33 ± 0.13	
	High State	$\mathrm{PL}_{\mathrm{baseline}} + \mathbf{PL}_{\mathbf{binary}}$	$(1.45 \pm 0.18) \times 10^{-12}$	1.00	2.73 ± 0.15	⋯	
	Pre-2017	$\mathbf{PL}_{\mathrm{baseline}}$	$(1.26 \pm 0.25) \times 10^{-14}$	3.39	2.14 ± 0.28	⋯	7.2/8
	Low State	$\mathrm{PL}_{\mathrm{baseline}} + \mathbf{PLEC}_{\mathrm{binary}}$	$(1.64 \pm 1.12) \times 10^{-11}$	0.56	0.65 ± 0.75	0.33 ± 0.13	
	High State	$\mathrm{PL}_{\mathrm{baseline}} + \mathbf{PLEC}_{\mathrm{binary}}$	$(1.20 \pm 0.41) \times 10^{-11}$	0.51	2.37 ± 0.50	2.39 ± 3.23	
MAGIC (>80 GeV)	Pre-2017	$\mathbf{PL}_{\mathrm{baseline}}$	$(2.04 \pm 0.63) \times 10^{-14}$	3.50	2.23 ± 0.17	⋯	9.6/12
	Fall 2017	$\mathrm{PL}_{\mathrm{baseline}} + \mathbf{PL}_{\mathbf{binary}}$	$(1.65 \pm 0.33) \times 10^{-12}$	0.70	2.61 ± 0.18	⋯	
	Pre-2017	$\mathbf{PL}_{\mathrm{baseline}}$	$(2.20 \pm 0.64) \times 10^{-14}$	3.50	2.17 ± 0.26	⋯	4.8/11
	Fall 2017	$\mathrm{PL}_{\mathrm{baseline}} + \mathbf{PLEC}_{\mathrm{binary}}$	$(3.77 \pm 1.68) \times 10^{-12}$	0.70	1.74 ± 0.37	1.40 ± 0.97	
	Pre-2017	$\mathbf{PL}_{\mathrm{baseline}}$	$(2.30 \pm 0.67) \times 10^{-14}$	3.50	2.15 ± 0.19	⋯	4.4/15
	Low State	$\mathrm{PL}_{\mathrm{baseline}} + \mathbf{PL}_{\mathbf{binary}}$	$(9.84 \pm 3.41) \times 10^{-13}$	0.70	2.57 ± 0.26	⋯	
	High State	$\mathrm{PL}_{\mathrm{baseline}} + \mathbf{PL}_{\mathbf{binary}}$	$(3.69 \pm 0.64) \times 10^{-12}$	0.70	2.17 ± 0.23	⋯	
	Pre-2017	$\mathbf{PL}_{\mathrm{baseline}}$	$(2.63 \pm 0.60) \times 10^{-14}$	3.50	2.06 ± 0.17	⋯	3.0/14
	Low State	$\mathrm{PL}_{\mathrm{baseline}} + \mathbf{PLEC}_{\mathrm{binary}}$	$(5.11 \pm 3.61) \times 10^{-12}$	0.70	1.55 ± 0.61	0.58 ± 0.33	
	High State	$\mathrm{PL}_{\mathrm{baseline}} + \mathbf{PL}_{\mathbf{binary}}$	$(1.65 \pm 0.14) \times 10^{-12}$	0.70	2.20 ± 0.40	⋯	
	Pre-2017	$\mathbf{PL}_{\mathrm{baseline}}$	*Insufficient data to discriminate between PL and PLEC in high state*				
	Low State	$\mathrm{PL}_{\mathrm{baseline}} + \mathbf{PLEC}_{\mathrm{binary}}$					
	High State	$\mathrm{PL}_{\mathrm{baseline}} + \mathbf{PLEC}_{\mathrm{binary}}$					

Note. Each group of rows shows the result of a simultaneous fit of both the baseline emission from the region prior to the appearance of the binary, modeled as a power law (PL), and the sum of this baseline with a new component from the binary, modeled as either a power law or a power law with an exponential cutoff (PLEC). These fits were performed across the data periods defined in Section 3. In each row, the parameters shown correspond to the model component listed in bold, where N_0 is the differential flux normalization (calculated at the de-correlation energy E_0), Γ is the spectral index, and E_C is the cutoff energy for PLEC models. The χ^2 and degrees of freedom (dof) are calculated from the joint fit across the given data.

sets, with the high and low states fit with the baseline power law plus either a pure power law or a power-law with an exponential cutoff. The VERITAS data favor a cutoff model in the low state, with an F-test probability of 0.999 and a cutoff value of 0.33 ± 0.13 TeV. MAGIC observations also favor a low-state cutoff model, with a probability of 0.980 and a cutoff value of 0.58 ± 0.33 TeV. For both observatories, the high-state data are well fit by a pure power law and including a cutoff does not significantly change the quality of the fit.

4. Discussion

PSR J2032+4127/MT91 213 is the second TeV gamma-ray binary system to be detected in which the nature of the compact object is clearly established. Non-thermal emission from these systems likely results from the interaction of the pulsar wind with the wind and/or disk of the Be star (Tavani & Arons 1997; Kirk et al. 1999; Dubus 2013). Particles are accelerated at the shock that forms between the pulsar and Be star winds. These subsequently produce synchrotron emission from radio to X-ray bands and inverse Compton emission at TeV energies. Numerous competing factors play a role in creating and modulating the observed emission. These include the efficiency of inverse Compton production and the degree of photon–photon absorption, which both depend upon the geometrical properties of the system with respect to the line of sight and the intensity, wavelength, and spatial distribution of target photon fields (Böttcher & Dermer 2005). Additional factors include: the position of the pulsar in relation to structures in the stellar wind (Petropoulou et al. 2018); the bulk motion and cooling of the post-shocked material (Dubus 2006); the structure of the magnetic field around the star (Sierpowska & Bednarek 2005); and the degree of magnetization of the pulsar wind and its evolution with radial distance from the pulsar (Takata & Taam 2009). Isotropized pair cascades, triggered by misaligned VHE photons that would not otherwise be observed, can also contribute to the emission (Bednarek 1997; Sushch & Böttcher 2014). Finally, interactions with the material and radiation of a circumstellar disk, the defining feature of the Be stellar class, may also modulate the X-ray and gamma-ray fluxes (Sierpowska-Bartosik & Bednarek 2008).

Modeling the time-dependent broadband emission is therefore complex and challenging. Takata et al. (2017) have presented a model that explains the increasing X-ray flux prior to periastron as the result of the radial dependence of the pulsar wind magnetization, and the X-ray suppression at periastron due to Doppler boosting effects caused by bulk motion of the post-shocked flow, naturally leading to an emission light curve that is asymmetric with respect to periastron. A recently revised version of their model predictions is given in Li et al. (2018), and also in Figure 1. The model prediction matches the early part of the XRT light curve reasonably well, when scaled by a factor of 0.5, but is unable to reproduce the rapid brightening around MJD 58080, when PSR J2032+4127/MT91 213 was at superior conjunction. This feature may be explained, at least in part, by interaction of the pulsar with the circumstellar disk of the Be star, which could be confirmed by observations of radio pulsations during the periastron passage. Alternatively, as discussed in Petropoulou et al. (2018), it may be caused by geometrical effects associated with the orientation of the stellar disk with respect to the pulsar's orbit.

Bednarek et al. (2018) also calculated gamma-ray emission from the system, including a detailed treatment of the pair cascades triggered by the absorption of primary gamma-rays, and the subsequent production of inverse Compton emission. They do not calculate a detailed light curve, but conclude that the binary emission may dominate the overall VHE flux, becoming comparable to, or exceeding, the steady flux from TeV J2032+4130 for a few weeks around periastron and superior conjunction. The predicted elevated flux close to periastron of $\sim 1.6 \times 10^{-12}$ erg cm^{-2} s^{-1} at 1 TeV is similar to the high-state emission levels reported in this Letter. We also note that the VHE efficiency ($L_{>200\,\mathrm{GeV}}/\dot{E} = 1.4\%$) for PSR J2032+4127/MT91 213 is approximately the same as that of PSR B1259–63/LS 2883. In contrast, the GeV efficiency of PSR J2032+4127/MT91 213 is significantly lower than that of PSR B1259–63/LS 2883, which can exceed 100% (Johnson et al. 2018; Li et al. 2018).

A distinctive feature observed in the VHE light curve is a sharp flux drop around seven days after periastron, lasting just a few days. As noted in Takata et al. (2017), a similar dip has been seen in the light curve of PSR B1259–63/LS 2883, which Sushch & van Soelen (2017) attributed to photon–photon absorption. This effect is predicted to be strongest when both the interaction angle between the photons is optimal and when the gamma-ray photons pass through the densest photon field, which occurs around superior conjunction, five to 15 days after periastron for PSR J2032+4127/MT91 213.

Based on the detailed sampling of the VHE and X-ray light curves reported here, coupled with the measurement of an unexpected low-energy spectral cutoff in the VHE low state, it is clear that the existing models will require significant revision. Analysis of the pulsar timing evolution over periastron will provide important additional input, including more accurate measurements of the system geometry. It will also allow for more sensitive searches for GeV emission in the *Fermi*-LAT data, with the dominant magnetospheric emission from the pulsar removed by a temporally gated analysis.

Finally, it is interesting to reconsider the properties of the steady VHE source, TeV J2032+4130, in the light of these results. As noted in Aliu et al. (2014), if we assume that TeV J2032+4130 is the PWN of PSR J2032+4127, then PSR J2032+4127 is one of the oldest and weakest pulsars with a nebula seen in both X-ray and VHE gamma-rays. In a recent population study, the Abdalla et al. (2017) derived empirical relations between VHE luminosity and pulsar spin-down energy, and also between PWN radius and characteristic age. For PSR J2032+4127, these relations predict a radius of over 20 pc (compared to a measured extent of 4.7×2.0 pc), and a TeV luminosity (1–10 TeV) of 2×10^{33} erg s^{-1} (compared to the measured value of 8×10^{32} erg s^{-1}). However, the measured properties of VHE PWN display a large intrinsic scatter, and the physical size of the nebula can be strongly modified by the local interstellar environment. We conclude that PSR J2032+4127 remains a plausible candidate for the power source driving TeV J2032+4130 and note that it may be worthwhile to search for extended TeV nebulae around other known TeV binary systems—although the formation of TeV J2032+4130 may only be possible due to the exceptionally long orbital period and large eccentricity of the binary system, which allows PSR J2032+4127 to spend much of its orbit effectively as an isolated pulsar.

X-ray and gamma-ray monitoring of PSR J2032+4127/MT91 213 will continue. PSR B1259–63/LS 2883 produces bright gamma-ray flares in the days and months after periastron, and it ejects rapidly moving plasma clumps generated by the interaction of the pulsar with the stellar disk (Pavlov et al. 2015). Similar phenomena may occur in the case of PSR J2032+4127/MT91 213. The ongoing observing campaigns therefore provide a rare opportunity to completely sample the high-energy behavior of this system around periastron, which will not be repeated until approximately 2067.

VERITAS is supported by the U.S. Department of Energy, the U.S. National Science Foundation, the Smithsonian Institution, and by NSERC in Canada. We acknowledge the excellent work of the support staff at the Fred Lawrence Whipple Observatory and at collaborating institutions in the construction and operation of VERITAS.

We acknowledge *Fermi* and *Swift* GI program grants 80NSSC17K0648 and 80NSSC17K0314.

The MAGIC Collaboration thanks the funding agencies and institutions listed in: https://magic.mpp.mpg.de/ack_201805.

Facilities: Swift-XRT, VERITAS, MAGIC.

Software: astropy (Astropy Collaboration et al. 2013), ROOT (Brun & Rademakers 1997), XSPEC (Arnaud 1996).

ORCID iDs

W. Benbow https://orcid.org/0000-0003-2098-170X
R. Bird https://orcid.org/0000-0002-4596-8563
A. Furniss https://orcid.org/0000-0003-1614-1273
G. H. Gillanders https://orcid.org/0000-0001-8763-6252
D. Hanna https://orcid.org/0000-0002-8513-5603
P. Kaaret https://orcid.org/0000-0002-3638-0637
D. Kieda https://orcid.org/0000-0003-4785-0101
M. Krause https://orcid.org/0000-0001-7595-0914
G. Maier https://orcid.org/0000-0001-9868-4700
R. Mukherjee https://orcid.org/0000-0002-3223-0754
A. N. Otte https://orcid.org/0000-0002-5955-6383
N. Park https://orcid.org/0000-0002-4282-736X
M. Pohl https://orcid.org/0000-0001-7861-1707
E. Pueschel https://orcid.org/0000-0002-0529-1973
G. T. Richards https://orcid.org/0000-0002-1408-807X
M. Santander https://orcid.org/0000-0001-7297-8217
I. Sushch https://orcid.org/0000-0002-2814-1257
D. A. Williams https://orcid.org/0000-0003-2740-9714

J. Becerra González https://orcid.org/0000-0002-6729-9022
W. Bednarek https://orcid.org/0000-0003-0605-108X
E. Bernardini https://orcid.org/0000-0003-3108-1141
M. Gaug https://orcid.org/0000-0001-8442-7877
F. Leone https://orcid.org/0000-0001-7626-3788
F. Longo https://orcid.org/0000-0003-2501-2270
P. Munar-Adrover https://orcid.org/0000-0002-1942-7376
A. Niedzwiecki https://orcid.org/0000-0002-8541-8849
M. Nievas Rosillo https://orcid.org/0000-0002-8321-9168
K. Nilsson https://orcid.org/0000-0002-1445-8683
S. Paiano https://orcid.org/0000-0002-2239-3373
M. Ribó https://orcid.org/0000-0002-9931-4557
L. Saha https://orcid.org/0000-0002-3171-5039
N. Sahakyan https://orcid.org/0000-0003-2011-2731
F. Tavecchio https://orcid.org/0000-0003-0256-0995

References

Abdalla, H., Abramowski, A., Aharonian, F., et al. 2017, A&A, 612, A2
Abdo, A. A., Ackermann, M., Ajello, M., et al. 2009, Sci, 325, 840
Abdo, A. A., Ackermann, M., Ajello, M., et al. 2011, ApJL, 736, L11
Abeysekara, A. U., Archer, A., Aune, T., et al. 2018, ApJ, 861, 134
Aharonian, F., Akhperjanian, A., Beilicke, M., et al. 2002, A&A, 393, L37
Aharonian, F., Akhperjanian, A., Beilicke, M., et al. 2005, A&A, 431, 197
Aharonian, F., Akhperjanian, A. G., Aye, K.-M., et al. 2005, A&A, 442, 1
Aharonian, F., Akhperjanian, A. G., Bazer-Bachi, A. R., et al. 2006, A&A, 460, 743
Albert, J., Aliu, E., Anderhub, H., et al. 2008a, ApJL, 675, L25
Albert, J., Aliu, E., Anderhub, H., et al. 2008b, NIMPA, 588, 424
Aleksić, J., Ansoldi, S., Antonelli, L. A., et al. 2016, APh, 72, 76
Aliu, E., Aune, T., Behera, B., et al. 2014, ApJ, 783, 16
Arnaud, K. A. 1996, in ASP Conf. Ser. 101, Astronomical Data Analysis Software and Systems V, ed. G. Jacoby & J. Barnes (San Francisco, CA: ASP), 17
Astropy Collaboration, Robitaille, T. P., Tollerud, E. J., et al. 2013, A&A, 558, A33
Bednarek, W. 1997, A&A, 322, 523
Bednarek, W., Banasiński, P., & Sitarek, J. 2018, JPhG, 45, 015201
Böttcher, M., & Dermer, C. D. 2005, ApJL, 634, L81
Brun, R., & Rademakers, F. 1997, NIMPA, 389, 81
Burrows, D. N., Hill, J. E., Nousek, J. A., et al. 2005, SSRv, 120, 165
Camilo, F., Ray, P. S., Ransom, S. M., et al. 2009, ApJ, 705, 1
Coe, M. J., Steele, I. A., Ho, W. C. G., et al. 2017, ATel, 10920, 1
Dubus, G. 2006, A&A, 456, 801
Dubus, G. 2013, A&ARv, 21, 64
Dubus, G., Guillard, N., Petrucci, P.-O., & Martin, P. 2017, A&A, 608, A59
Fomin, V. P., Stepanian, A. A., Lamb, R. C., et al. 1994, APh, 2, 137
Gaia Collaboration 2018, A&A, 616, A1
Hillas, A. M. 1985, Proc. ICRC 1985 (San Diego, CA), 19, 445
Ho, W. C. G., Ng, C.-Y., Lyne, A. G., et al. 2017, MNRAS, 464, 1211
Johnson, T. J., Wood, K. S., Kerr, M., et al. 2018, ApJ, 863, 27
Johnston, S., Manchester, R. N., Lyne, A. G., et al. 1992, ApJL, 387, L37
Kirk, J. G., Ball, L., & Skjæraasen, O. 1999, APh, 10, 31
Krawczynski, H., Carter-Lewis, D. A., Duke, C., et al. 2006, APh, 25, 380
Li, K. L., Kong, A. K. H., Tam, P. H. T., et al. 2017, ApJ, 843, 85
Li, K. L., Takata, J., Ng, C. W., et al. 2018, ApJ, 857, 123
Lyne, A. G., Stappers, B. W., Keith, M. J., et al. 2015, MNRAS, 451, 581
Maier, G., & Holder, J. 2017, Proc. ICRC (Busan), 35, 747
Negueruela, I., Ribó, M., Herrero, A., et al. 2011, ApJL, 732, L11
Park, N. & The VERITAS Collaboration 2015, Proc. ICRC (The Hague), 34, 771
Pavlov, G. G., Hare, J., Kargaltsev, O., Rangelov, B., & Durant, M. 2015, ApJ, 806, 192
Petropoulou, M., Vasilopoulos, G., Christie, I. M., Giannios, D., & Coe, M. J. 2018, MNRAS, 474, L22
Sierpowska, A., & Bednarek, W. 2005, MNRAS, 356, 711
Sierpowska-Bartosik, A., & Bednarek, W. 2008, MNRAS, 385, 2279
Sushch, I., & Böttcher, M. 2014, JHEAp, 3, 18
Sushch, I., & van Soelen, B. 2017, ApJ, 837, 175
Takata, J., & Taam, R. E. 2009, ApJ, 702, 100
Takata, J., Tam, P. H. T., Ng, C. W., et al. 2017, ApJ, 836, 241
Tavani, M., & Arons, J. 1997, ApJ, 477, 439
VERITAS & MAGIC Collaborations 2017, ATel, 10810, 1
Zanin, R., Carmona, E., Sitarek, J., et al. 2013, Proc. ICRC (Rio de Janeiro), 33, 773